Solid State Communications 151 (2011) 97–101

Contents lists available at ScienceDirect

Solid State Communications

journal homepage: www.elsevier.com/locate/ssc

Ferromagnetic behavior of high-purity ZnO nanoparticles

R. Escudero *, R. Escamilla

Instituto de Investigaciones en Materiales, Universidad Nacional Autónoma de México, A. Postal 70-360, México, D.F. 04510, Mexico

ARTICLE INFO

Article history:
Received 28 October 2010
Received in revised form
10 November 2010
Accepted 16 November 2010
by P. Sheng
Available online 21 November 2010

Keywords:
A. ZnO nanoparticles
C. Core–shell structure
D. Ferromagnetism

ABSTRACT

ZnO nanoparticles with the wurtzite structure were prepared by chemical methods at low temperature in aqueous solution. The size of the nanoparticles is in the range from about 10 to 30 nm. Ferromagnetic properties were observed from 2 K to room temperature and above. Magnetization versus temperature, $M(T)$, and isothermal $M(H)$ measurements were obtained. The coercive field clearly shows ferromagnetism above room temperature. An exchange bias was observed, and we related this behavior to the core–shell structure present in the samples. The chemical synthesis, structure, and defects in the bulk related to oxygen vacancies are the main factors for the observed magnetic behavior.

1. Introduction

Recently, zinc oxide, ZnO, has attracted intense interest because of its possible application in distinct technological fields: spintronics, magnetic semiconductors, catalysts, sensors, field emission devices, solar cells, etc. [1]. This compound is a band gap semiconducting material with a direct band gap of 3.37 eV, and electronic concentration only about 10^{12} to 10^{14} cm^{-3}. In bulk material, the zinc atoms occupy the special position 2b with coordinates (1/3, 2/3, 0), and the oxygen atoms also occupy special position 2b with coordinates (1/3, 2/3, u), where $u = a/c$ $(3/8)^{1/2} = 0.3817$; see [2]. Fig. 1 presents the hexagonal structure characteristic of ZnO. The ZnO wurtzite structure, also known as the mineral zincite, has cell parameters $a = 3.249$ Å and $c = 5.206$ Å, consistent with the standard JCPDS 36–1451 diffraction pattern card.

In addition to studies in bulk crystalline material, nanoparticles of this compound with different morphologies have become important for the reason that the electronic characteristics may change at the nanometric scale [3–8]. These changes are mainly related to the volume/area ratio, V/A, which may result in different physical characteristics and behavior. Recently, studies of native point defects in ZnO bulk by Anderson and Van de Walle [9] have described the influence of defects on the electronic properties. In compounds at the nanometric scale, the ratio V/A changes the physical and chemical properties, making different electronic mechanisms possible. Many workers in the field of nanomaterials have used different procedures for the preparation of this material; they have used various physical and chemical techniques to synthesize this compound [4,10]. In this work, we prepared the nanostructured material using a sol–gel method, as described by Ma et al. [11]. The nanostructures obtained present interesting new magnetic characteristics, some of which have already been reported by other authors; see [8,6,7]. In this paper, we present studies concerned with structural defects in ZnO nanomaterials and the magnetic ordering found. Our observation shows that ZnO of size from about 10–30 nm presents ferromagnetic ordering up to room temperature, which can be related to vacancies of oxygen or Zn atoms [12]. X-ray photoelectron spectroscopy (XPS) measurements confirm that vacancies are an important factor.

2. Experimental details

Nanoparticles of ZnO were prepared using the sol–gel method. Different amounts of dihydrated zinc acetate, $Zn(CH_3COO)_2$ (Aldrich 99.99%), was used as the precursor, and it was diluted in deionized water at pH = 7 and 25 °C; ammonium hydroxide, (NH_4OH), was added slowly as a dispersive medium, with the following reaction taking place:

$$Zn(CH_3COO)_2 + 2NH_4OH \rightarrow Zn(OH)_2 + 2CH_3COO^- + 2NH_4^+.$$

The resulting gel was dried at 60 °C in air for about 30 h, and subsequently annealed in air, at a maximum temperature between 200 and 300 °C depending on the precursor amount, to obtain ZnO. The reaction is

$$Zn(OH)_2 \rightarrow ZnO + H_2O.$$

Different ZnO powder samples were prepared using distinct pH values and precursor amounts [13]. In this paper we will mainly

* Corresponding author. Tel.: +5255 5622 4625.
E-mail address: escu@servidor.unam.mx (R. Escudero).

0038-1098/$ – see front matter © 2010 Elsevier Ltd. All rights reserved.
doi:10.1016/j.ssc.2010.11.019

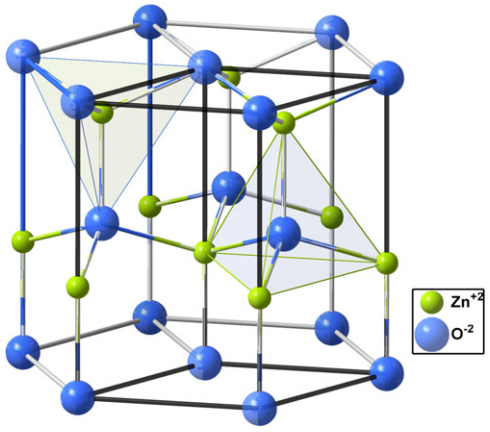

Fig. 1. (Color online) Wurzite crystalline structure of ZnO. In this figure, the two tetrahedra show a different configuration for the anions and cations: one shows a cation as the central atom whereas the another shows the anion surrounded by four cations at the corners. This coordination forms a typical sp^3 covalent bonding.

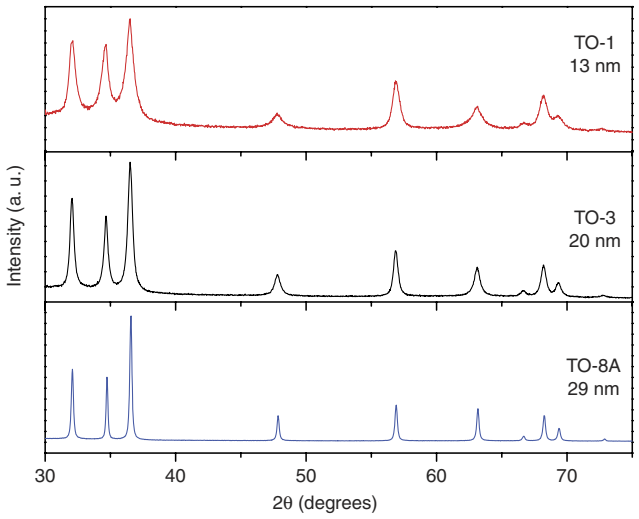

Fig. 2. (Color online) X-ray powder diffraction data for the three samples. The panels show the effect of the size of the nanoparticles. From top to bottom: 13, 20, and 29 nm. The powder spectra for all nanopowders correspond to a pure structure without impurities, and the data correspond to the wurtzite hexagonal structure.

describe the resulting study done on three samples: TO-1, TO-3, and TO-8A. The samples were characterized and analyzed by X-ray diffraction, as shown in Fig. 2. There we present the X-ray diffraction patterns for the three ZnO samples. The panels show the X-ray spectra from nanoparticles with average size from about 30–13 nm; the size was determined from the Scherrer formula, using a Gaussian fit. All the diffraction peaks were appropriately indexed, and they correspond with the hexagonal wurtzite ZnO structure.

Phase identification was performed by using a Brucker D8 X-ray diffractometer with Cu K_α radiation and a Ni filter. Intensities were measured at room temperature in steps of 0.025°, in the 2θ range 6° to 130°. The crystallographic phases were identified by comparison with the X-ray pattern of the JCPDS database. The parameters were refined with a Rietveld fit program, Rietica v 1.71, with multi-phase capability [14]. The structural parameters for samples TO-1, TO-3, and TO-8A are given in Table 1. We include the R_p, R_e, and R_{wp} data related to the Rietveld fitting. Chemical analysis was carried out by X-ray photoelectron spectroscopy (XPS). The analysis was performed using a VG Microtech ESCA 2000 Multilab UHV system, with an Al K_α X-ray source, $h\nu = 1486.6$ eV, operated at 15 kV and with a 20 mA beam, and a CLAM4 MCD analyzer (Fig. 3).

Table 1
Structural parameters for ZnO at 295 K.

Sample	3	1	8A
a (Å)	3.2504(1)	3.2501(2)	3.2507(4)
c (Å)	5.2113(1)	5.2213(3)	5.2076(6)
V (Å^3)	47.68	47.76	47.66
u	0.3820	0.3812	0.3823
N (Zn)	1.00(1)	1.00(1)	1.00(3)
N (O)	0. 97(4)	0.98(4)	1.00(2)
B_{iso} (Å^2):Zn	0.34(3)	0.29(4)	0.29(4)
B_{iso} (Å^2):O	1.70(3)	2.10(4)	1.92(4)
R_p (%)	10.20	8.90	16.1
R_e (%)	4.19	4.20	3.98
R_{wp} (%)	12.84	11.8	20.78
GoF	3.07	2.8	5.2

Note. Space group: $P6_3mc$ (# 186). N is the occupancy factor. Atomic positions: Zn: 2b (1/3, 2/3, 0); O: 2b (1/3, 2/3, u), where $u = (a/c)(3/8)^{1/2}$.

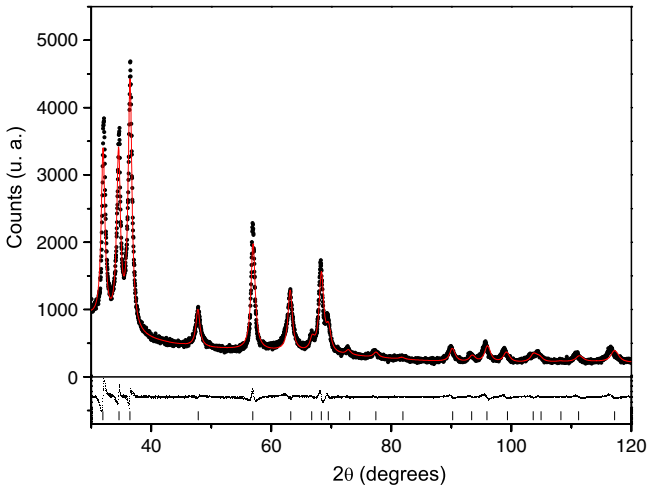

Fig. 3. (Color online) Rietveld refining data for the 20 nm sample corresponding to the wurtzite hexagonal structure. The crystalline structure in our samples is related to deficiencies of oxygen or metal atoms in the structure.

In order to perform the analysis, the surfaces of pellets of the material were etched with Ar^+ for 20 min with 4.5 kV at 0.3 μA mm^{-2}. The XPS spectrum was obtained at 55° with respect to the normal surface, with a constant energy mode pass (CAE), at $E_0 = 50$ and 20 eV for the survey and high-resolution narrow scan, respectively. The atomic relative sensitivity factor (RSF) reported by Scofield was corrected by the transmission function of the analyzer [15] and by ZnO as reference material. The peak positions were referenced to the background silver $3d_{5/2}$ photopeak at 368.21 eV, having a full width at half maximum (FWHM) of 1.00 eV, and C 1s hydrocarbon groups in the 284.50 eV central peak position. The XPS spectra were fitted with the program SDP v 4.1 [16].

Transmision electron microscopy (TEM) micrographs were obtained with a JEOL FEG 2010 FASTEM analytical microscope. The X-ray and TEM investigations showed that nanoparticles with size below 15 nm present a light grey color, whereas those with size above 25 nm have a normal white coloration. TEM images of the samples are displayed in Fig. 4. It is interesting to see a core–shell structure that surrounds the nanoparticles, delimiting the bulk and the surface. This feature has also been observed by Karmakar et al. [17]. We assume that these structural features may be related from the thermodynamical point of view to the decrease of the ground-state energy of the ZnO nanoparticles. As we will explain below, the magnetic characteristics can also be affected by this core–shell structure. One possibility is that the magnetic ordering in the bulk and on the surface is different. If this hypothesis is

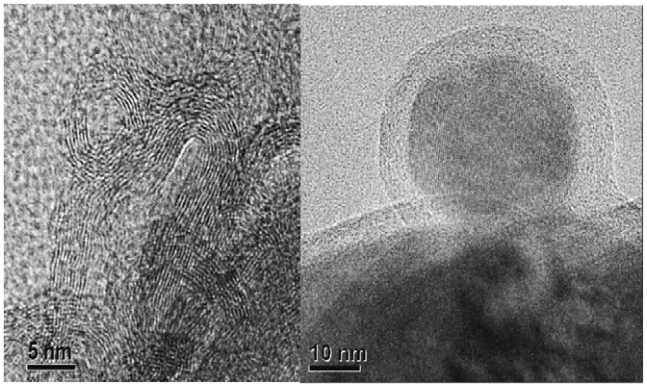

Fig. 4. Transmision electron microscopy (TEM) images of ZnO nanoparticles. The TEM images display the size of typical nanoparticles. Note the core–shell structure observed. We suggest that this feature of the nanoparticles is responsible for the exchange bias magnetic behavior.

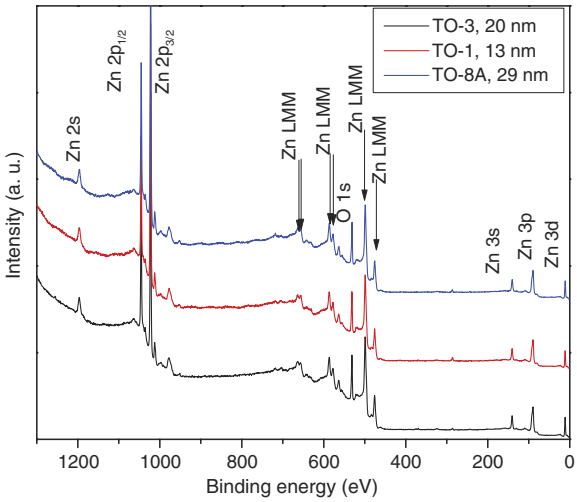

Fig. 5. (Color online) XPS survey spectra after Ar^{+} etching of polycrystalline samples TO-1, TO-3, and TO-8A. No extra peaks corresponding to any magnetic impurity were observed. Only Zn and O atoms are present, without other transition metal impurities.

correct the behavior would be observed as an exchange bias in the coercive field features.

In order to examine the stoichiometry of the compound, we analyzed the samples by X-ray photoelectron spectroscopy (XPS). Fig. 5 shows the XPS survey spectra after Ar^{+} etching on the samples. No extra peak related to any magnetic impurities was observed.

Fig. 6(a) shows the deconvolution of the XPS spectra in the O 1s region for samples TO-3 and TO-8A. The asymmetric O 1s peak in the surface was fitted by three Lorentzian–Gaussian components, centered at 529.90 eV, 530.42 eV, and 531.96 eV, respectively. The three fitted binding energy peaks approximate the results of Chen et al. [18] and Wang et al. [19]. Chen et al. attributed the peak on the low binding energy side of the O 1s spectrum to the O^{2-} ions in the wurtzite structure of the hexagonal Zn^{2+} ion array, surrounded by zinc atoms with the full supplement of nearest-neighbor O^{2-} ions. Accordingly, this peak of the O 1s spectrum can be attributed to the Zn–O bonds. The higher binding energy at 531.96 eV is usually attributed to chemisorbed or/and dissociated oxygen and OH species on the surface of the ZnO thin film (such as CO_3, adsorbed H_2O or O_2 [18,20]). The component at the medium binding energy of the O 1s peak may be associated with O^{2-} ions existing in oxygen-deficient regions within the ZnO matrix. Thus, as a result, changes in the intensity of this component may be in

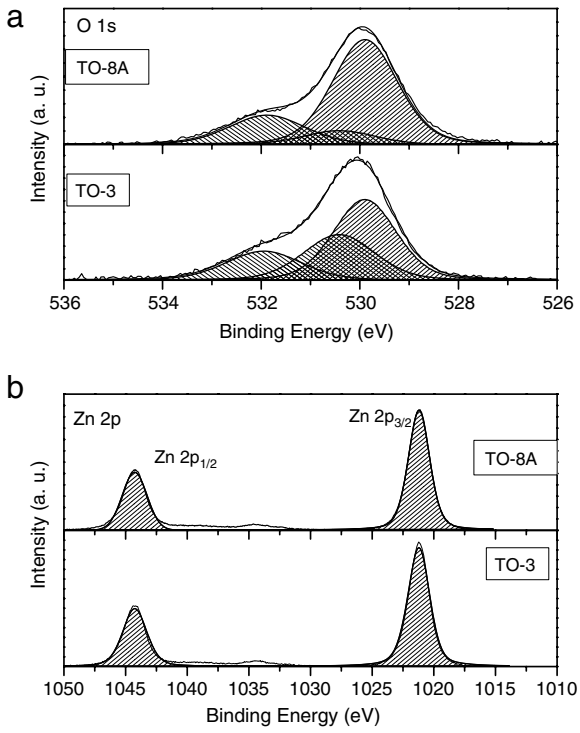

Fig. 6. High-resolution XPS spectra of the (a) O 1s and (b) Zn 2p core levels for two polycrystalline samples, TO-3 and TO-8A. The detailed shape is fitted assuming the contributions for three components belonging to two different chemical states of the ZnO bulk sample. The lower binding energy component at 529.90 eV is attributed to the structure of hexagonal Zn^{+2}. The medium and higher binding energy components at 530.42 and 531.96 eV are assigned to oxygen deficiencies in ZnO.

connection with the variations in the concentration of the oxygen vacancies [21]. The intensity of the peak localized at 529.90 eV exceeds those at 530.42 and 531.96 eV, indicating the strong Zn–O bonding in ZnO.

In order to determine the sample compositions, the atomic concentration was calculated by XPS using the survey spectra and the RSF values for O 1s and Zn 2p, 2.95 and 9, respectively. For the three samples studied, TO-8A, TO-3 and TO-1, the percentage of atomic oxygen was determined as 0.757, 0.736, and 0.715, respectively. Fig. 6(b) shows the deconvolution of the XPS spectra in the Zn 2p region for these samples. The Zn 2p spectrum shows a doublet, whose binding energies are 1021.21 and 1044.26 eV, which can be identified as the lines Zn-$2p_{3/2}$ and Zn-$2p_{1/2}$, respectively. The binding energy differences between the two lines is 22.4 eV, which is comfortably lying close to the standard reference value of ZnO [22]. The values of binding energy and binding energy difference, calculated from the XPS study, show that the Zn atoms are in the Zn^{2+} oxidation state. No metallic Zn with a binding energy of 1021.5 eV was observed [23]. This confirms again that Zn is in the Zn^{2+} state. Furthermore, at this stage is not possible to determine the presence of Zn interstitial defects from the Zn 2p spectra; these may be established only by the Auger peak of Zn.

2.1. Magnetic characteristics

The magnetic behavior was investigated from low temperature, 2 K, to room temperature. The characteristics were determined by using an MPMS Quantum Design Magnetometer. Magnetization versus temperature $M(T)$ measurements were obtained with magnetic field intensities of 1 and 50 kOe, and in two typical modes of measurement, to determine possible irreversible effects. In zero-field cooling (ZFC) mode, the sample is first cooled to the minimum

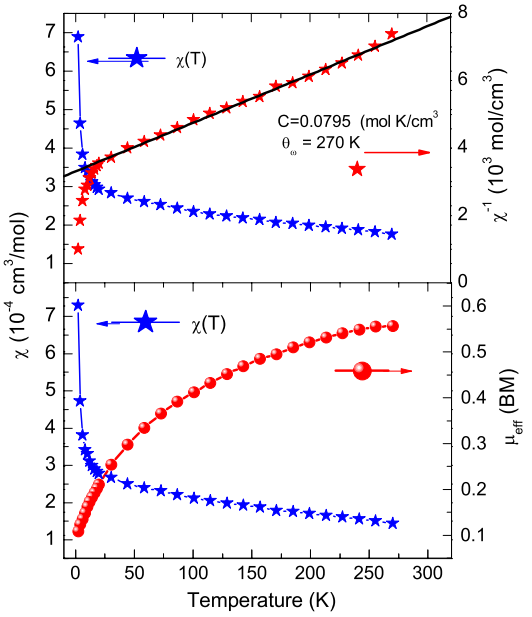

Fig. 7. (Color online) The top panel displays the magnetic susceptibility, $\chi(T)$. The left axis is $\chi(T)$ in terms of cm^3/mol. The behavior is of Curie–Weiss type. The right axis shows the inverse susceptibility: the full line indicates the fitting values of $C = 0.0795$ mol K cm^3, and $\theta_\omega = -270$ K. In the lower panel we also present other typical data for $\chi(T)$, with Curie constant $C = 0.055$ mol K cm^3; the number of Bohr magnetons is shown at the right, with a room-temperature value of only 0.55.

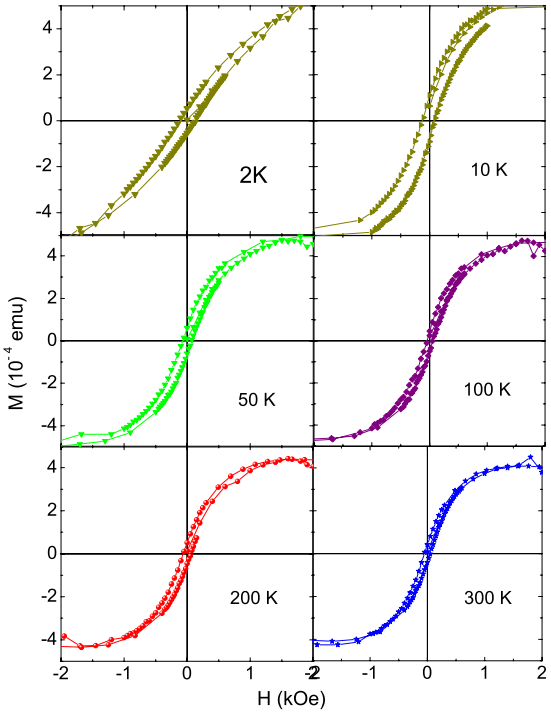

Fig. 8. (Color online) Isothermal measurements, $M(H)$, at six different temperatures displaying a coercive field which is large at low temperature and decreasing as the temperature increases. In addition, an exchange bias was observed.

accessible temperature. Once in thermal equilibrium, the magnetic field is applied and the measurement is initiated, increasing the temperature. In field-cooling (FC) mode, the measurement is performed starting at the maximum temperature with the magnetic field applied, and decreasing the temperature. With those two modes, the behavior related to irreversible processes can readily be observed. In addition to these measurement, we also obtained measurements at the two mentioned different magnetic intensities to observe possible metamagnetic effects; in all measurements neither metamagnetic or irreversibility processes were observed. Fig. 7 displays a typical susceptibility characteristic as a function of temperature, for two different size particle samples measured at two distinct fields. In general we observed similar magnetic behavior for all samples, with small variation of the Curie constant from about 0.05 to 0.09 mol K/cm^3, and with small change of the Weiss temperature from about -250 to -326 K. Such small Curie constant values are quite representative of a very weak ferromagnetic behavior. Fig. 7 displays both sets of data in two different samples. The top panel also shows the inverse susceptibility $\chi^{-1}(T)$ fitting very well to a Curie–Weiss behavior from high temperature to below 50 K. The resulting Curie constant is $C = 0.0795$ mol K cm^3, and the Weiss temperature $\theta_\omega = -270$ K. The bottom panel shows $\chi(T)$, and the right axis shows that the number of Bohr magnetons, μ_{eff}, at room temperature is about 0.55, a value that is similar for all samples. This behavior is indicative of a geometric frustrated system [24] with a frustrated parameter close to 1 defined as $f = \theta_\omega/T_C$, for T_C above 300 K.

In order to have better insight about the magnetic behavior of the ZnO samples, we obtained isothermal magnetization measurements from 2 K to above room temperature to characterize the resulting coercive fields. Fig. 8 shows $M(H)$ at six different temperatures. In Fig. 9, we show that at all temperatures there exists a coercive field, with an exchange bias. At 2 K, it has a low value with respect to the value at 5 K; this decreases as the temperature increases above 5 K in a smooth form up to 200 K. It seems that above 250 K another small anomalous change occurs, and this followed for a smooth decrease up to reach room temperature and

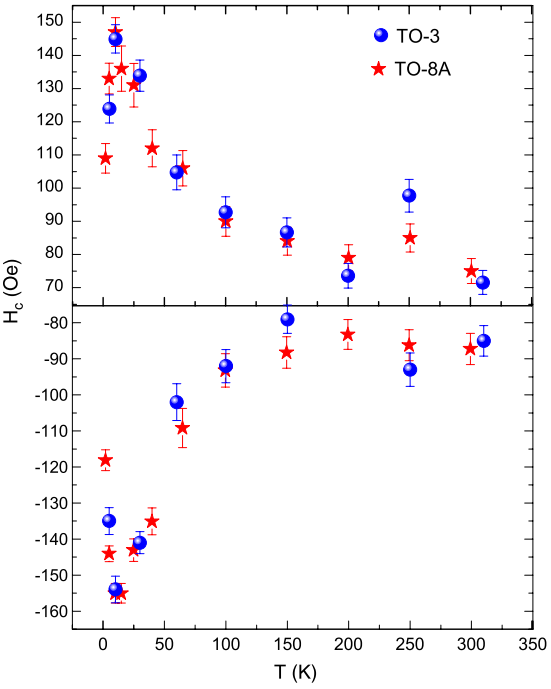

Fig. 9. (Color online) Plots of the coercive field, displaying a exchange bias. This exchange bias behavior may be related to the influence of the core–shell structure of the ZnO nanoparticles.

above. We have plotted in Fig. 9 the positive and negative parts of the coercive field. One can clearly see the small but different coercive field in the samples, and also in the negative and positive parts. We speculate that this exchange bias may be related to two possible magnetic orderings, one existing on the surface and other in the bulk. The core–shell characteristics of our samples are very possibly related to this behavior [25]. However, we do not have a complete explanation for the two observed anomalous peaks of

the coercive field at low temperature and high temperature. It is important to stress the purity of the samples. In particular, we did not find detect any magnetic impurities.

3. Conclusions

In this experimental study of ZnO nanoparticles prepared using a sol–gel method, we demonstrate that ferromagnetism exists up to room temperature. Rietveld refining shows that the cell parameters are almost similar to those of bulk samples. XPS studies show the presence of oxygen vacancies, with an amount around 25–29%. As was mentioned before by Panchakarla et al. [3], the occurrence of ferromagnetism in nanoparticle oxides seems to be a general phenomenon that can be attributed to oxygen vacancies and to the volume/area ratio. The surface of those structures, with different amounts of vacancies, also changes the magnetic behavior. In this study, the observed core–shell morphology in our nanoparticles clearly explains the exchange bias in the isothermal measurements. The core–shell structure as seen by other researchers affects the magnetism of the nanoparticles.

Acknowledgements

We thank F. Silvar for helium provision, L. Huerta for XPS measurements, L. Rendon for high-resolution TEM measurements, L. Diazbarriga for help in the conclusion of this study, and O. Garcia and A. Fernandez for help with the initial method of sample preparation. We acknowledge DGAPA grant No. IN100711.

References

[1] U. Ozgur, Ya.I. Alivov, C. Liu, A. Teke, M.A. Reshchikov, S. Dogan, V. Avrutin, S.J. Cho, H. Morkoc, J. Appl. Phys. 98 (2005) 041301.
[2] Erich H. Kisi, Margaret M. Elcombe, Acta Crystallogr. C 45 (1989) 1867.
[3] L.S. Panchakarla, Y. Sundarayya, S. Manjunatha, A. Sundaresan, C.N.R. Rao, Chem. Phys. Chem. 11 (2010) 1673.
[4] Yanhe Xiao, Liang Li, Yan Li, Ming Fang, Lide Zhang, Nanotechnology 16 (6) (2005) 671.
[5] Hui Zhang, Deren Yang, Xiangyan Ma, Yujie Ji, Jin Xu, Duanlin Que, Nanotechnology 15 (2004) 622.
[6] A. Sundaresan, R. Bhargavi, N. Rangarajan, U. Siddesh, C.N.R. Rao, Phys. Rev. B 74 (2006) 161306 (R).
[7] A. Sundaresan, C.N.R. Rao, Solid State Commun. 149 (2009) 1197.
[8] Nguyen Hoa Hong, Joe Sakai, Virginie Brizé, J. Phys.: Condens. Matter 19 (2007) 036219.
[9] Anderson Janotti, Chris G. Van de Walle, Phys. Rev. B 76 (2007) 165202.
[10] Hulan Zhou, Zhuang Li, Mater. Chem. Phys. 89 (2005) 326.
[11] Xiangyang Ma, Hui Zhang, Yujie Ji, Jin Xu, Deren Yang, Mater. Lett. 59 (27) (2005) 3393.
[12] Kay Potzger, Shengqiang Zhou, Phys. Status Solidi B 246 (6) (2009) 1147.
[13] A.A. Ismail, A. El-Midany, E.A. Abdel-Aal, H. El Shall, Mater. Lett. 59 (2005) 1924.
[14] C.J. Howard, B.A. Hunter, D.A.J. Swinkels Rietica, IUCR Powder Diffr. 22 (1997) 21.
[15] J.H. Scofield, J. Electron Spectrosc. 8 (1976) 129.
[16] SDP, v4.1 (32 bit) Copyright 2004, XPS International, LLC, Compiled, January 2004.
[17] Debjani Karmakar, S.K. Mandal, R.M. Kadam, P.L. Paulose, A.K. Rajarajan, T.K. Nath, A.K. Das, I. Dasgupta, G.P. Das, Phys. Rev. B 75 (2007) 144404.
[18] M. Chen, X. Wang, Y.H. Yu, Z.L. Pei, X.D. Bai, C. Sun, R.F. Huang, L.S. Wen, Appl. Surf. Sci. 158 (2000) 134.
[19] Z.G. Wang, X.T. Zu, S. Zhu, L.M. Wang, Physica E 35 (2006) 199.
[20] S. Major, S. Kumar, M. Bhatnagar, K.L. Chopra, Appl. Phys. Lett. 49 (1986) 394.
[21] T. Szörényi, L.D. Laude, I. Bertóti, Z. Kántor, Z. Geretovszky, J. Appl. Phys. 78 (1995) 6211.
[22] C.D. Wagner, W.M. Riggs, et al., Handbook of X-ray Photoelectron Spectroscopy, Perkin Elmer, Eden Prairie, 1979.
[23] M.N. Islam, T.B. Ghosh, K.L. Chopra, H.N. Acharya, Thin Solid Films 280 (1996) 20.
[24] A.P. Ramirez (Ed.), Handbook of Magnetic Materials, in: Geometrical Frustration, vol. 13, Elsevier Science B.V., 2001, (Chapter 4).
[25] J. Nogues, I.K. Schuller, J. Magn. Magn. Mater. 192 (1999) 203.